ACS APPLIED MATERIALS & INTERFACES

Research Article

www.acsami.org

Highly Alloyed PtRu Nanoparticles Confined in Porous Carbon Structure as a Durable Electrocatalyst for Methanol Oxidation

Chunzhen Yang,* Ming Zhou, and Liang Gao

Department of Chemistry, The University of Hong Kong, Pokfulam Road, Hong Kong SAR, Hong Kong

Supporting Information

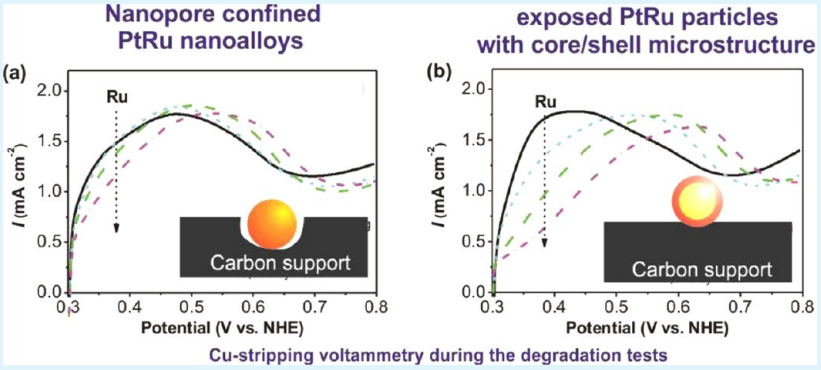

ABSTRACT: The state-of-the-art carbon-supported PtRu catalysts are widely used as the anode catalysts in polymer electrolyte fuel cells (PEMFCs) but suffer from instability issues. Severe ruthenium dissolution occurring at potentials higher than 0.5 V vs NHE would result in a loss of catalytic activity of PtRu hence a worse performance of the fuel cell. In this work, we report an ultrastable PtRu electrocatalyst for methanol oxidation by confining highly alloyed PtRu nanoparticles in a hierarchical porous carbon structure. The structural characteristics, e.g., the surface composition and the morphology evolution, of the catalyst during the accelerated degradation test were characterized by the Cu-stripping voltammetry and the TEM/SEM observations. From the various characterization results, it is revealed that both the high alloying degree and the pore confinement of PtRu nanoalloys play significant roles in suppressing the degradation processes, including Ru dissolution and particle agglomeration/migration. This report provides an opportunity for efficient design and fabrication of highly stable bimetallic or trimetallic electrocatalysts in a large variety of applications.

KEYWORDS: *PtRu electrocatalysts, Ru dissolution, pore confinement, polymer electrolyte fuel cells, catalyst degradation, stability*

1. INTRODUCTION

Bimetallic catalysts, composed of two metal elements in either alloy or intermetallic form, have emerged as materials of a new category with promising catalytic properties for many electrocatalytic applications.[1,2] In particular, Pt-based bimetallic catalysts supported on high surface area carbon have received extensive investigations as electrode materials for polymer electrolyte membrane fuel cells (PEMFCs).[3,4] For example, alloys with the general formula Pt_3X (where X is a 3d transition metal, such as Ni, Co, Fe, and etc.) give high activity toward oxygen reduction reaction (ORR).[5,6] However, in the acidic fuel cell environment, dissolution of the base metal in the oxidized form from the surface of bimetallic catalysts remains a major problem of concern in this field.[7−10] Both theoretical predictions and experimental observations have shown that a strong metal leaching can occur during the fuel cell operation.[11,12] Developing a rational strategy to mitigate metal dissolution is still subject to insightful investigation.

Among the bimetallic materials, PtRu particles supported on carbon have been developed as a state-of-the-art electrocatalyst toward methanol oxidation reaction (MOR) based on the "bifunctional" mechanism.[13,14] In a recent review, Antolini summarized the problems of Ru dissolution from Pt−Ru catalysts during the fuel cell operation. Moreover, it has been pointed out that suppressing Ru dissolution is a key challenge to improve the stability and durability of the anodic PtRu/C catalysts in an acidic environment.[10] Indeed, the presence of the Ru dissolution from PtRu catalyst lowers not only the catalytic activity but also the CO tolerability.[15−19] Besides these negative effects, the leached Ru can penetrate through the polymer electrolyte membrane and then redeposit at the cathode.[20] This would significantly inhibit the kinetics of oxygen reduction and largely limit the capability of the cathode on handling the methanol crossover. In this case, the overall cell voltage could decrease by an order of 40−200 mV. In addition, the process involving Ru dissolution from the PtRu surface in the anode and the deposition on the cathode is irrecoverable.[15,20,21] To solve these problems, several strategies have been proposed,

Received: July 22, 2014
Accepted: October 3, 2014
Published: October 3, 2014

Scheme 1. Schematic Illustration of the Structural Features of (a) PtRu@CS with Highly Alloyed PtRu Nanoparticles Uniformly Distributed and Confined in Nanopores of Carbon Texture and (b) PtRu/CS with PtRu Nanoparticles in a Pt-Rich Core/Ru-Rich Shell Microstructure Deposited on the External Surface of Carbon Support

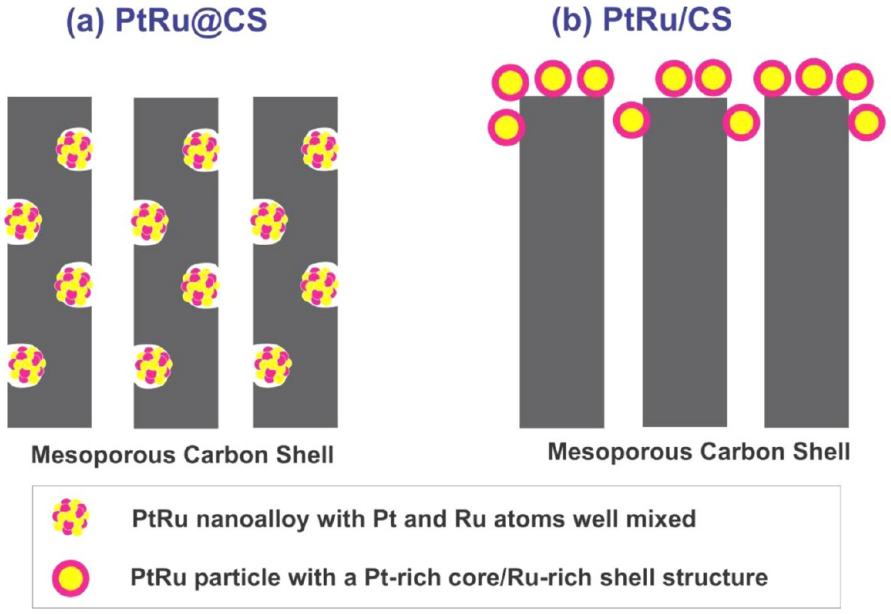

such as the use of suitable supports[21−23] or the presence of stabilizing agents[24] (e.g., the addition of gold to the PtRu catalyst[8]). Despite the considerable effort in this field, however, the positive effects from these methods on the above-mentioned problems are limited.

Recent investigations have shown that a high alloying degree could be crucial for the stabilization of PtRu catalysts with a low Ru dissolution in acidic media.[10,17,25−27] Gancs et al.[26] investigated the effect of alloying degree of PtRu catalysts on CO and methanol electrooxidation. Interestingly, it was found that a high alloying degree of PtRu was beneficial for maintaining the anodic activity in a prolonged operation time. Yamada et al.[17] found that Pt-enriched-core/Ru-enriched-shell structure was instable. The enriched Ru species on the surface are easily crystallized in a hexagonal close-packed (hcp) phase and are likely to be dissolved preferentially in the early stage of a durability test.[10] Thus, it is desirable to drive the Ru species into the Pt phase to reduce the formation of the hcp phase. In this aspect, the formation of PtRu alloy is considerably related to the preparation method. Up to now, PtRu/C catalysts have been obtained by various synthetic strategies, such as the polyol method,[28−32] microemulsion method,[33−35] spray pyrolysis method,[36] coimpregnation method,[27,37] and coprecipitation method,[38] etc. In these methods, a Pt-enriched-core/Ru-enriched-shell structure is typically formed probably due to the different reduction rates of the two metals in the solution. As mentioned above, this structure with Ru enriching on the surface is unfavorable for the catalyst stability.[30,39]

To improve the alloying degree of the PtRu catalyst, a post heat-treatment appears to be attractive since the formation of the PtRu alloy is easier to proceed, as demonstrated by Antolini et al.[40] However, high temperature would inevitably result in aggregation of metal particles. If the particles can be confined to migrate at high temperatures, the aggregation can be reduced, while the alloying degree of PtRu can be improved simultaneously. In this respect, we recall the pore confinement effect, which has been used to improve the stability of Pt particles toward ORR. The confinement of Pt particles inside the pores can suppress Pt particle migration/agglomeration and Pt detachment from carbon support.[41,42] However, uniformly dispersing well-mixed bimetallic PtRu nanoparticles into the nanopores is a challenging issue. To our knowledge, investigation of the nanopore confinement effect toward the degradation of PtRu catalysts, especially the process of Ru dissolution, has not yet been reported thus far.

Herein, we demonstrated a surfactant-free synthetic route for uniformly confining PtRu nanoparticles in the porous carbon structure. More importantly, due to the postheat-treatment process, the obtained PtRu nanoparticles are highly alloyed. For comparison, we also synthesize a carbon-supported PtRu catalyst using the well-known "polyol" method, following the process reported in the literature.[31,32] To achieve a high catalytic activity, carbon spheres with hollow core−mesoporous shell (HCMS) structure are employed as carbon support in this work. The hierarchical HCMS structure with interconnected bimodal pore system of the carbon support can facilitate the mass transfer of methanol molecules and other electrolyte ions during the MOR, and hence the catalytic activity of the supported PtRu catalysts is expected to be enhanced. Scheme 1 illustrates the structural features of the as-synthesized PtRu catalysts. Degradation behaviors of the synthesized PtRu catalysts, as well as a commercially available PtRu catalyst, were studied by accelerated degradation tests (ADTs) with up to 8000 repeated potential scans within a potential range of 0−0.6 V vs NHE in blank H_2SO_4 electrolyte. Cu-stripping voltammetry was conducted after given cycles of potential scans to monitor the loss of electrochemically active surface area (ECSA) and surface Ru concentration. Morphology changes of the decayed catalysts were studied by TEM. Results of this work will provide fundamental understandings for the degradation behaviors of carbon-supported PtRu catalysts and, to a great extent, facilitate the development of highly efficient electrocatalysts with applicable stability.

2. EXPERIMENTAL SECTION

2.1. Synthesis of the Exposed PtRu Catalyst by the "Polyol" Method. PtRu nanoparticles supported on carbon spheres were synthesized via the "EG" method and denoted as PtRu/CS. The synthetic process was illustrated by Route A in Scheme S1 (Supporting Information). Using solid core−mesoporous shell (SCMS) silica spheres (core diameter, 300 nm; shell thickness, 80 nm, Figures S1 and S2, Supporting Information) as the hard template, HCMS carbon spheres with a core diameter of 260 nm and a shell thickness of ca. 50 nm were prepared (Figure S3, Supporting Information) and then employed as carbon support. A solution of furfuryl alcohol (0.28 mL) and oxalic acid as catalyst with a molar ratio of 30:1 was added to SCMS silica spheres (0.6 g) with the incipient-wetness impregnation method. The composites were heated at 80 °C for 3 h and then at 160 °C for 3 h in air for the polymerization of furfuryl alcohol. Then the resultants were annealed in a tube furnace at 700 °C for 3 h under argon atmosphere for carbonization. SiO_2 templates were etched from the silica/carbon composites using a 10 wt. % hydrofluoric acid (HF) solution. The obtained carbon spheres were cleaned repeatedly with water and ethanol and then dried in an oven.

The obtained HCMS carbon spheres (78 mg) were added to an ethylene glycol solution (EG) containing H_2PtCl_6 (13.3 mg of Pt) and $RuCl_3$ (6.7 mg of Ru) with a pH value of 13 set with NaOH in EG (0.5 M). The above mixture was then heated at 210 °C for 4 h. After cooling, the pH was set at 5 by adding HCl solution (0.1 M). After stirring overnight, the products were collected by centrifugation and cleaned repeatedly. The resulting PtRu/CS catalyst was dried at 60 °C in an oven.

2.2. Synthesis of the Pore-Confined PtRu Catalyst. The synthetic approach is schematically illustrated in Scheme S1 (Supporting Information) (Route B), and the resulting catalyst is denoted as PtRu@CS. In general, 0.6 g of the above-mentioned SCMS silica spheres was suspended in dry CH_2Cl_2 (80 mL), to which an aqueous solution (0.28 mL) containing H_2PtCl_6 and $RuCl_3$ (8.84 mg of Pt and 4.4 mg of Ru) was added dropwise under vigorous stirring. Upon filtration, the powder was collected and dried in vacuum oven at 60 °C. An amount of 0.28 mL of furfuryl alcohol was impregnated into the above SCMS silica composite stored in a refrigerator. The as-synthesized composites were kept at 60 °C in an oven for 24 h and then carbonized in a tube furnace at 700 °C for 3 h under argon atmosphere. The silica spheres were etched with a 5 wt % HF solution. The obtained PtRu catalyst was cleaned with deionized water and ethanol repeatedly and dried at 60 °C in an oven.

2.3. Characterization Techniques. Scanning transmission electron microscopy (STEM, Philips TECNAI 20 with a 200 kV accelerating voltage) and field emission scanning electron microscopy (SEM, Hitachi S-4800 FEG) were employed to characterize the morphology and structure of the synthesized PtRu catalysts. Energy-dispersive X-ray spectroscopy (EDX) was obtained with STEM equipped with INCAx-sight EDX detectors (Oxford Instruments) to determine the composition of the synthesized PtRu catalysts. Powder X-ray diffraction (XRD) spectra were obtained on a PANalytical X-ray diffractometer using Cu Kα radiation (λ = 0.1541 nm) at a sweeping rate of 2 deg/min. Thermogravimetric analysis (TGA) was performed in air with a PERKIN ELMER TGA-7 Thermogravimetric Analyzer to determine the metal load. Nitrogen sorption isotherms were obtained with a Micromeritics ASAP 2020 analyzer at 77 K to evaluate the surface area, pore volume, and pore size distribution of the synthesized samples. The surface area was determined by the Brunauer−Emmett−Teller (BET) method, and the pore size distribution was calculated by the Barrett−Joyner−Halenda (BJH) method.

2.4. Electrochemical Measurements. Electrochemical measurements were performed with a Solatron SI1287 potentiostat. A three-electrode configuration was used with a Pt plate as the counter electrode, Ag/AgCl as the reference electrode, and a glassy carbon (GC) electrode (from Pine Instruments) with an area of 0.196 cm^2 as the working electrode. The GC thin-film electrode was prepared in a three-step method. Carbon-supported PtRu catalyst (4.0 mg) was dispersed into a solution containing 2-proponal (900 μL) and Nafion solution (0.5 wt %, 100 μL), followed by ultrasonic treatment for 20 min, and then the resultant suspension (ca. 20 μL) was pipetted onto the GC electrode and dried at 60 °C for 1 h.

Cyclic voltammetry was carried out to study the methanol oxidation reaction (MOR) in an electrolyte containing 0.5 M H_2SO_4 and 1 M CH_3OH between 0.05 and 1.0 V (vs NHE) at a scan rate of 10 mV s^{-1} at room temperature (24 °C). Prior to each cyclic voltammetry measurement, the electrolytic solution was purged with pure N_2 for 30 min to remove the dissolved oxygen. All potential values in this work were normalized by the normal hydrogen electrode (NHE).

The ECSA and the surface composition of the catalysts were determined by Cu-stripping voltammetry.[43,44] The test electrode was immersed in 0.5 M H_2SO_4 solution containing 200 mM $CuSO_4$, and the potential was maintained at 0.3 V for 120 s to form a Cu monolayer on the PtRu surface. Linear sweep voltammetry was then performed from 0.3 to 0.8 V at 10 mV s^{-1}. As shown in eq 1, the charges associated with the Cu-stripping process are 420 μC cm^{-2}.

$$Cu^{2+} + 2e^- \rightarrow Cu_{UPD} \rightarrow Cu^{2+} + 2e^- \quad (1)$$

The underpotential deposited Cu was stripped from Ru sites at a potential region of 0.3−0.5 V vs NHE, lower than the second Cu oxidation peak from Pt sites (0.5−0.75 V vs NHE). The Cu-stripping wave was fitted with two Gaussian-like curves and integrated. The surface Ru composition of the PtRu catalysts (θ_{Ru}) was calculated based on the ratio of the integrated Cu-stripping charge at the Ru site (Q_{Ru}) to the total Cu-stripping charge (Q_{total}) according to eq 2[43]

$$\theta_{Ru} = \frac{Q_{Ru}}{Q_{total}} \times 100 \text{ (at. \%)} \quad (2)$$

The durability measurement was performed by repeated potential cycling in the range of 0−0.6 V with a scan rate of 50 mV s^{-1} in a 0.5 M H_2SO_4 electrolyte at room temperature (24 °C). Following the durability measurement, the electrode was removed from the H_2SO_4 solution, rinsed with deionized water, and characterized by Cu-stripping voltammetry.

3. RESULTS AND DISCUSSION

3.1. Characterization of the PtRu Electrocatalysts. The synthesis of the PtRu@CS catalyst was carefully monitored by SEM to confirm that all PtRu NPs were uniformly confined in the mesoporous carbon textures. Figure S4 (Supporting Information) shows the SEM images of the PtRu/carbon/silica composites after carbonization and the resulting PtRu@CS catalyst after removing the silica template. Isolated carbon

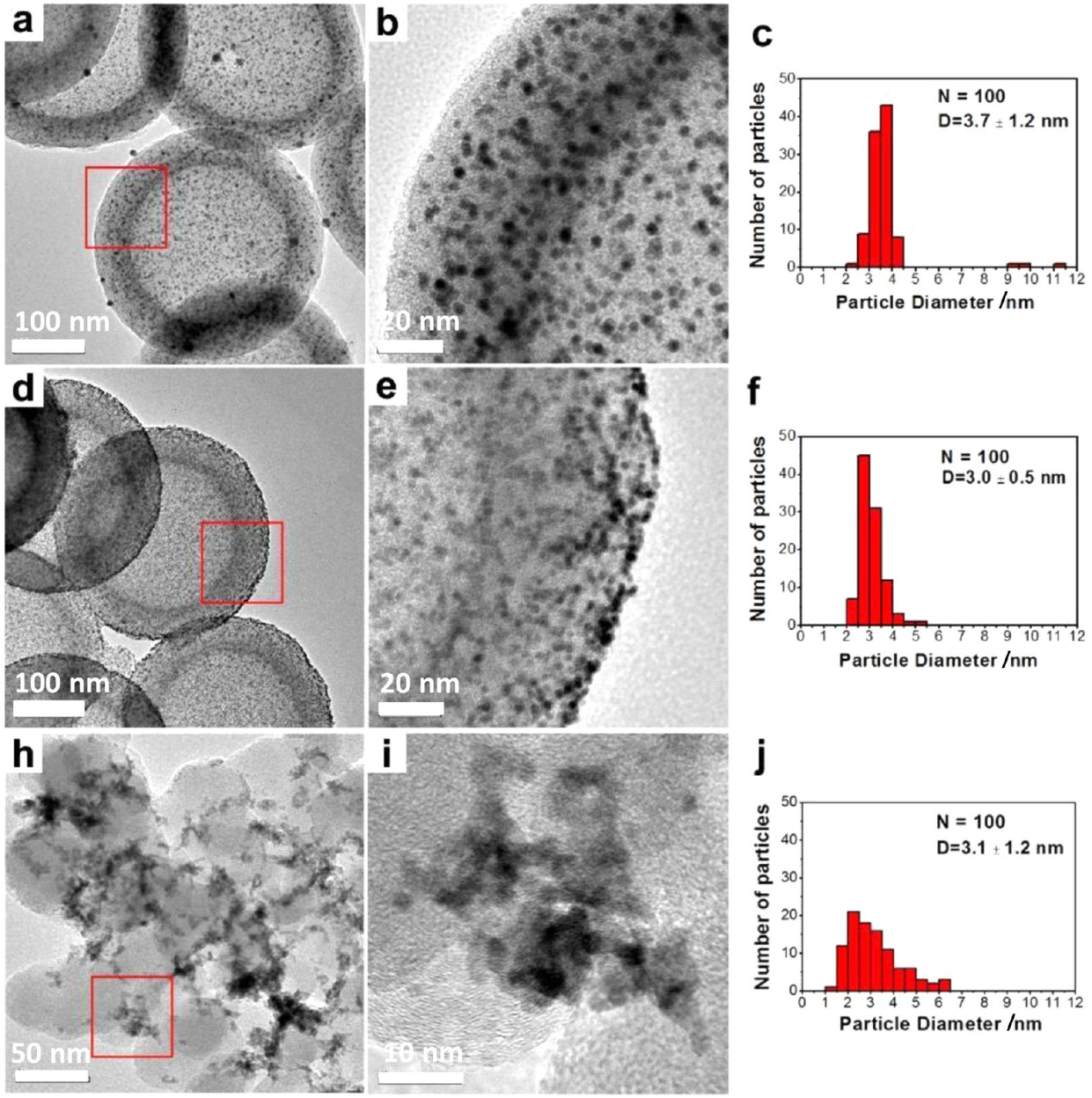

Figure 1. TEM images and the corresponding particle size distribution histograms of the PtRu catalysts: (a, b, c) for PtRu@CS; (d, e, f) for PtRu/CS; and (h, i, j) for PtRu/VC from E-TEK.

spheres with hollow cores of ca. 260 nm were observed, with a few metal particles located on the external carbon surface. Considering that the PtRu@CS catalyst was thermally treated at 700 °C for the carbonization of impregnated poly(furfuryl alcohol), the resulting PtRu nanoparticles were thus confined in the nanopores of HCMS carbon support, rather than situated at the external boundary of the carbon shells. Moreover, it is also expected that a high alloying degree can be obtained due to this thermal treatment process.

The carbon structure and metal dispersion of the examined PtRu catalysts were characterized by TEM (Figure 1). Both of the synthesized PtRu catalysts supported on the carbon spheres retained the same HCMS hierarchical structure, with macroscopic hollow cores of ca. 260 nm in diameter and mesoporous shells of ca. 50 nm in thickness. However, the metal dispersion of the two catalysts was rather different. The PtRu@CS exhibited a uniform dispersion of PtRu particles throughout the hierarchical carbon texture, with all PtRu nanoparticles confined inside the mesoporous carbon shells. The corresponding EDX elemental maps of Pt, Ru, and C (Figure 2) further confirmed that all Pt and Ru atoms were well-mixed and homogeneously distributed throughout the carbon support. In contrast, most PtRu particles of the PtRu/CS catalyst were located on the external surface of carbon support with slight agglomeration. This is in agreement with the previous study that the polyol method is not favorable for Pt particles to enter the porous channels of ordered mesoporous carbons (OMCs). Instead, the majority of Pt NPs is exposed on the external surface of carbon particles.[45] The difference in the metal particle dispersion between the PtRu@CS and PtRu/CS catalysts could possibly lead to different electrochemical performance. The histograms of PtRu particle size distribution showed that the average particle sizes were 3.7, 3.0, and 3.1 nm for PtRu@CS, PtRu/CS, and the E-TEK catalyst, respectively.

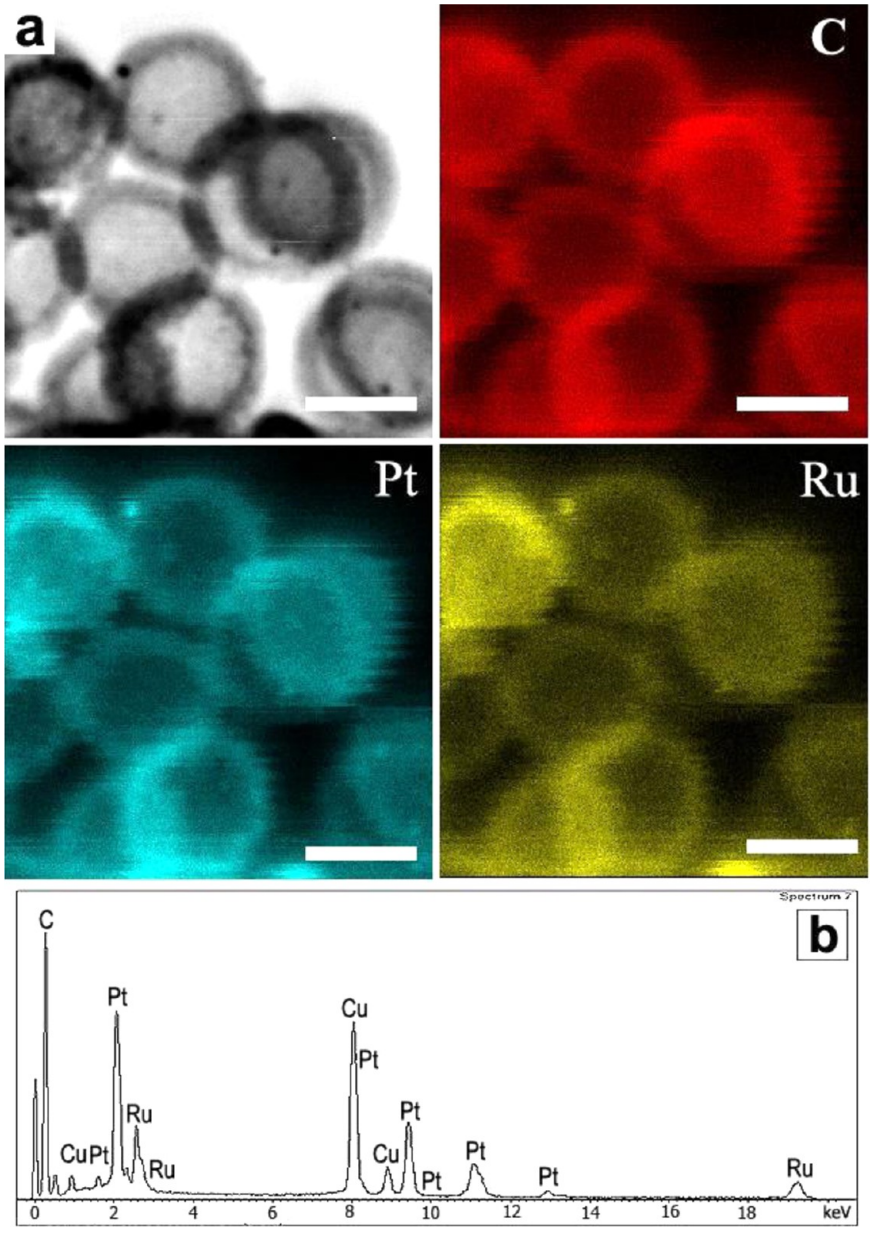

Figure 2. (a) Energy-dispersive X-ray spectroscopic (EDX) elemental maps of Pt, Ru, and C (Scale bar = 200 nm). (b) EDX result of the PtRu@CS catalyst.

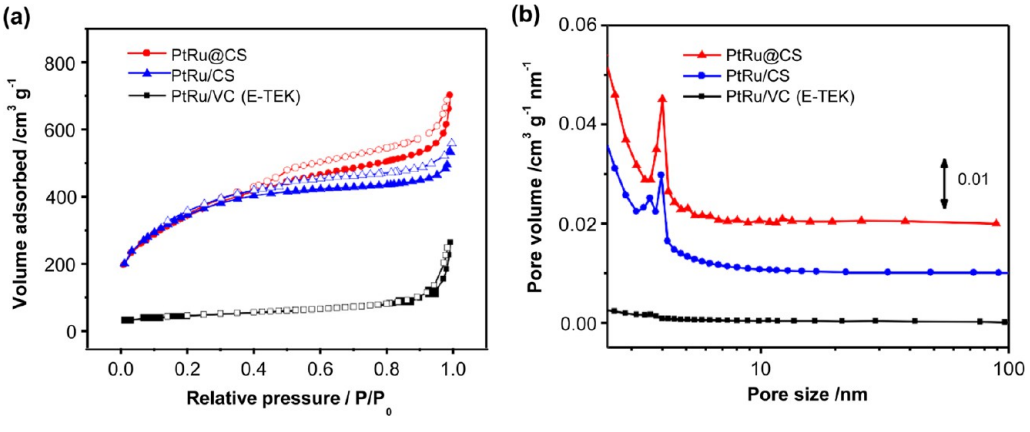

Figure 3. (a) N_2 sorption isotherms and (b) pore size distributions of the PtRu catalysts.

Table 1. Structural Parameters of the Synthesized PtRu Catalysts

samples	C^a/nm	S^a/nm	metal loading^b/wt %	BET surface area^c/m^2 g^{-1}	pore volume^c/cm^3 g^{-1}	pore diameter^c/nm
PtRu@CS	264 ± 10	55 ± 4	23.4	994.0	0.71	3.9
PtRu/CS	260 ± 12	53 ± 3	21.7	871.5	0.62	3.9
PtRu/VC (E-TEK)	–	–	20	154.6	0.24	–

[a]The diameters of the macrohollow cores (C) and the mesoporous shell thickness (S) of the HCMS carbon spheres were measured based on the TEM characterization. [b]PtRu metal load was determined by the TGA analysis. [c]BET surface area, pore volume, and pore diameter were measured by N_2 sorption isotherms.

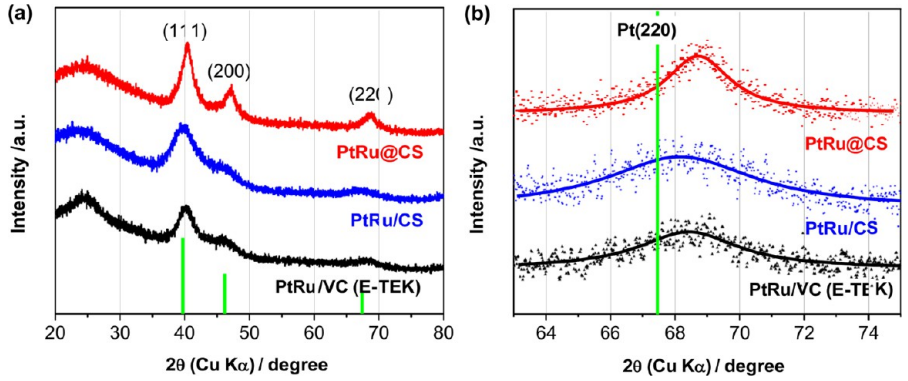

Figure 4. (a) XRD patterns of the PtRu catalysts: PtRu@CS, PtRu/CS, and E-TEK PtRu/VC. (b) Curve fitting results for the Pt(220) diffraction peaks.

Table 2. Peak Position of Pt(220) and Calculated Structural Parameters Based on the XRD Data

samples	(220) peak position (deg)	lattice parameter (Å)	bulk Pt:Ru composition (atom)^a	x_{Ru}	alloying degree (%)	particle size (nm)
PtRu@CS	68.69	3.862	1:1	0.43	77	4.2 ± 0.3
PtRu/CS	68.14	3.889	1:0.81	0.21	34	3.1 ± 0.4
PtRu/VC (E-TEK)	68.52	3.870	1:1.04	0.36	55	3.4 ± 0.3

[a]Bulk Pt:Ru composition was determined by EDX analyses.

The porosity of the HCMS carbon support was examined by N_2 adsorption/desorption (Figure 3). The BET surface area, pore volume, and pore size distribution (by BJH method) of various samples were derived and summarized in Table 1. Compared with PtRu/VC (E-TEK), the PtRu catalysts supported on HCMS carbon spheres exhibited higher surface areas (>800 m^2/g) and larger pore volume, which can enhance the electrochemical activity of PtRu due to more facile mass transportation. It is noted that the mesoporosity of PtRu@CS is higher than that of the PtRu/CS. This can be ascribed to the existence of abundant nanopores confining PtRu nanoparticles in the carbon structure. Both PtRu@CS and PtRu/CS showed similar pore size distribution curves (centered at 3.9 nm), suggesting that the carbon replica in both the PtRu@CS and the PtRu/CS catalysts shared a similar mesostructure.

The crystalline structure of the PtRu metal particles was studied by XRD (Figure 4). A broad peak at 2θ = 25° was observed in all X-ray diffractograms, which resulted from the graphitic carbon support.[46] All XRD patterns show three characteristic diffraction peaks of face-centered cubic structure of Pt crystal, which can be assigned to the (111), (200), and (220) planes. Moreover, all the observed XRD peaks slightly shifted toward higher values of 2θ due to the formation of the PtRu alloy. The diffraction peaks of the PtRu@CS catalyst at 2θ = 40° are relatively sharper than that of PtRu/CS, indicating relatively larger particle sizes of the formed PtRu particles. Antolini et al. have proposed that the alloying degree of the PtRu catalyst is defined by the Ru atomic fraction in the PtRu alloy.[40,47] The Pt(220) profiles from 63° to 75° (2θ) were fitted using the Lorentzian function with a linear background. The lattice parameters were calculated by indexing the (220) reflections and then used to estimate alloying degree of PtRu nanoparticles according to the following equations based on Vegard's law[48−50]

$$a = \frac{\sqrt{2}\lambda_{K\alpha 1}}{\sin\theta_{max}} \quad (3)$$

$$a = a_0 - 0.124x_{Ru} \quad (4)$$

$$\text{degree of alloying (\%)} = \frac{x_{Ru}}{[(1 - x_{Ru})(Ru/Pt)_{nom}]} \times 100 \quad (5)$$

where χ_{Ru} is the Ru atomic fraction in the PtRu alloy and $(Ru/Pt)_{nom}$ is the nominal Ru/Pt atomic ratio measured by EDX. The calculated alloying degree was 77% for PtRu@CS, 34% for PtRu/CS, and 55% for the E-TEK catalyst (as summarized in Table 2). Considering that the average particle size of PtRu was ca. 3.7 nm estimated from the TEM characterization, the heat treatment of the PtRu@CS catalyst at 700 °C during the carbonization step did not cause serious sintering or aggregation of PtRu nanoparticles. Instead, the alloying degree of the obtained PtRu catalyst was enhanced. Since there were no distinct diffraction peaks related to hexagonal close-packed Ru or tetragonal RuO_2 phases, the unalloyed Ru is probably in amorphous states.

Cu-underpotential deposition (UPD) stripping voltammetry is the preferred method for determining the surface area and

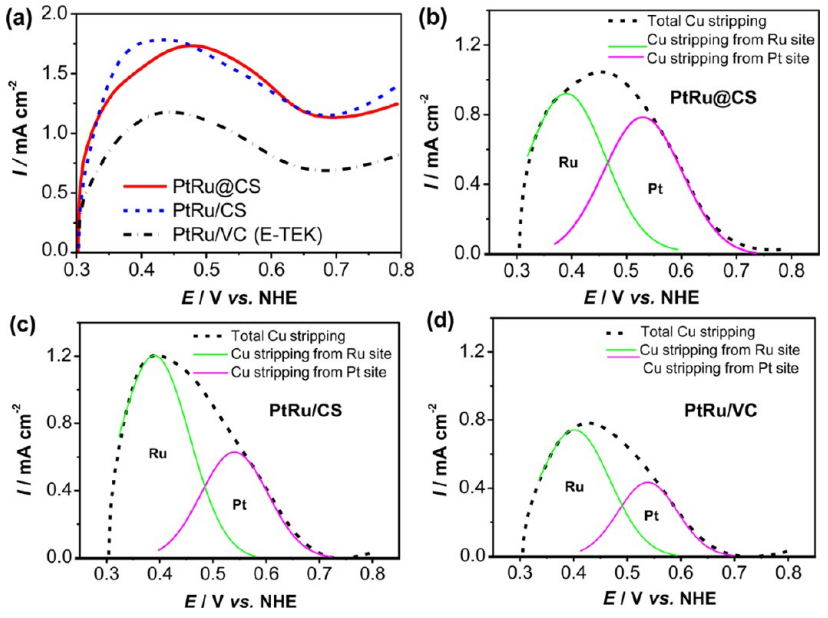

Figure 5. (a) Cu-stripping voltammograms of the examined PtRu catalysts and the corresponding curve-fitting results for (b) PtRu@CS, (c) PtRu/CS, and (d) PtRu/VC from E- TEK. (Capacitive contribution from the carbon support was subtracted as the background.)

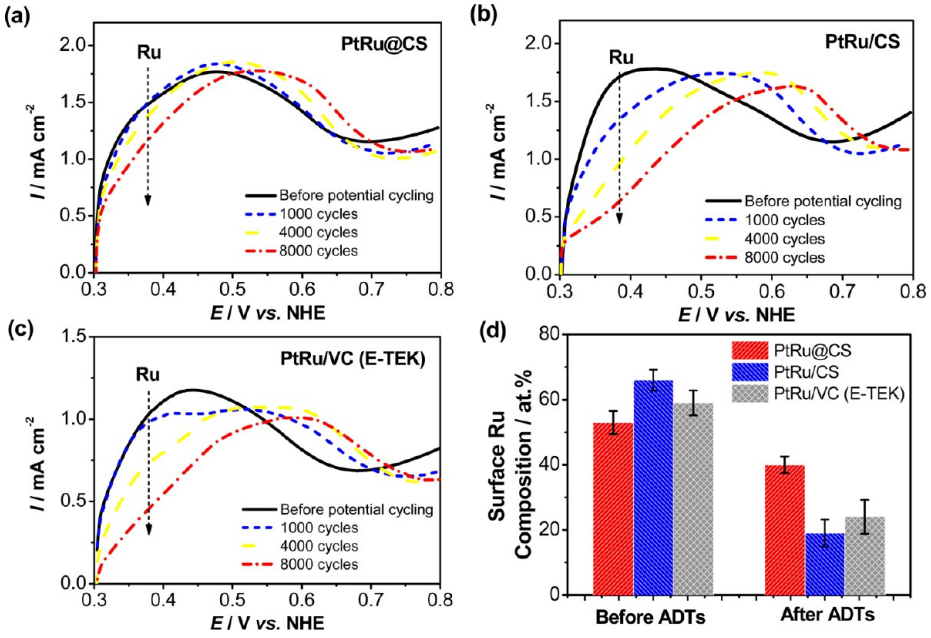

Figure 6. Ru dissolution process studied by the Cu-stripping voltammograms of the PtRu catalysts during the ADTs: (a) for PtRu@CS, (b) for PtRu/CS, and (c) for PtRu/VC from E-TEK. (d) Change of surface Ru composition for each PtRu catalyst during the degradation tests. The error bars reflect the standard deviations involved in the peak fitting.

surface compositions of PtRu electrodes. Because of the similarity of the atomic radii of the metals (Cu, 0.128 nm; Pt, 0.138 nm; Ru, 0.134 nm), the ratios of Cu deposited to Pt and to Ru are estimated to be 1:1. This permits a simple calculation of the total electrochemically active surface area for all three electrodes (Pt, Ru, and PtRu). Anthony et al. measured the surface area of the unsupported PtRu catalyst by the CO, Cu, and H UPD-stripping method, respectively, and found that the Cu-stripping measurement produced a value much closer to that determined from the BET analysis.[43,44] However, some caution must be taken since the Cu underpotential deposition and subsequent oxidation processes are dependent upon many factors of the catalysts. The surface compositions of the PtRu catalysts can be estimated from the Cu-stripping voltammetry by deconvoluting the oxidation curve into two peaks. The first peak is due to stripping of the deposit from surface ruthenium sites; however, a small contribution may arise from Pt (as seen from Figure S5, Supporting Information). The second peak reflects removal from Pt sites only. However, deconvolution of the Cu-stripping peaks to distinguish Pt and Ru sites may introduce additional errors.

The Cu-stripping method for the durability studies of PtRu catalysts was first validated using the Pt/VC (E-TEK) catalyst as a standard. The ECSAs of Pt after certain numbers of degradation scans were estimated from both H-desorption peaks and Cu-stripping voltammetry, as shown in Figure S5

Table 3. Bulk and Surface Compositions of the PtRu Catalysts before and after ADTs

	before ADTs			after ADTs		
catalyst	ECSA[a] (m^2 g^{-1} of PtRu)	surface composition Pt:Ru[b] (atom)	bulk composition Pt:Ru[c] (atom)	ECSA[a] (m^2 g^{-1} of PtRu)	surface composition Pt:Ru[b] (atom)	bulk composition Pt:Ru[c] (atom)
PtRu@CS	86	1:∼1.10	1:1	80	1:∼0.66	1:0.50−0.74
PtRu/CS	93	1:∼1.94	1:0.81	64	1:∼0.23	1:0.11−0.27
PtRu/VC	67	1:∼1.44	1:1.04	44	1:∼0.31	1:0.16−0.34

[a]ECSA of each examined PtRu catalyst was measured by Cu-stripping voltammetry assuming the charges associated with the Cu-stripping process were 420 μC cm^{-2}. [b]Surface composition was estimated from the Cu-stripping voltammetry. [c]Bulk composition was determined by the EDX analysis.

(Supporting Information). The close values of the ECSAs of Pt and the similarity of the decaying trend clearly suggest that the Cu-stripping voltammetry is a reliable method for the degradation studies of Pt-based electrocatalysts.

The surface compositions of these PtRu catalysts were determined by the Cu-stripping voltammetry (Figure 5). The Cu-stripping peak derived from the Ru atoms appeared in the potential region of 0.3−0.5 V, whereas that derived from the Pt atoms appeared in the region of 0.5−0.75 V.[43,44,51] It can be recognized that the Cu oxidation curves contributed from the Pt and Ru surface are slightly different for the three PtRu catalysts examined, indicating the presence of difference in their surface compositions. The surface Pt:Ru atomic ratio was calculated by deconvoluting the Cu-stripping curve with two Gaussian-like curves as demonstrated in Figure 6b−6d. The calculated PtRu atomic ratios are summarized in Table 3. It is noticed that the nominal Pt to Ru ratio was estimated close to 1 for the PtRu@CS catalyst, which is in good agreement with the results from the EDX analyses. Since both the bulk and surface compositions were close to $Pt_{50}Ru_{50}$, it is concluded that the Pt and Ru were well mixed in the nanoalloy. As for the PtRu/CS sample synthesized via the traditional EG method, the surface Ru composition was higher than Pt, deviating from its bulk composition measured by EDX. Therefore, the Pt and Ru components were not uniformly distributed in the particles prepared via the EG method, and the catalyst surface was enriched with Ru species. A microstructure of the Pt-enriched core/Ru-enriched shell was formed, mainly due to the reduction of Pt salt at a faster rate than that of the Ru salt in solutions. This is a major drawback of the polyol synthetic method as mentioned above. The commercial Vulcan carbon-supported PtRu catalyst also exhibited a Ru-rich surface as revealed from the Cu-stripping voltammetry shown in Figure 5d.

The ECSA of each PtRu catalyst was also calculated from the Cu-stripping voltammograms assuming that a monolayer of Cu atoms was deposited on the PtRu surface and the charge involved was 420 μC cm^{-2}. The PtRu/CS exhibited an ECSA of 93 m^2 g^{-1}, higher than that of PtRu@CS (86 m^2 g^{-1}). The higher ECSA value of the EG sample could be ascribed to the smaller particle sizes (∼3.0 nm) and easy accessibility of the electrolyte to the fully exposed PtRu nanoparticles. The ECSA of Vulcan carbon-supported PtRu/VC catalyst was 67 m^2 g^{-1}, which was probably due to the agglomeration of metal particles, as observed from the TEM characterization (Figure 1).

3.2. Accelerating Degradation Tests (ADTs). In order to investigate the electrochemical stability, ADTs with repeated potential cycling in the potential range of 0−0.6 V vs NHE up to 8000 cycles were performed in a 0.5 M H_2SO_4 electrolyte. The potential sweeping rate was maintained at 50 mV s^{-1}. This accelerated degradation test led to the decay of electrocatalysts.[52,53] Cu-stripping voltammograms were recorded for each electrode after given numbers of potential cycles. Figures 6a−6c show the evolution of Cu-stripping voltammograms of the examined PtRu catalysts with increasing degradation cycles. The small loss of Ru together with a slight increase in Pt portion was observed for the PtRu@CS catalyst. Both the ECSA and the surface Ru composition were well preserved during the whole degradation test, suggesting a remarkable electrochemical stability of the PtRu@CS catalyst. In contrast, the Cu oxidation curve from Ru sites between 0.3 and 0.5 V rapidly decreased in both PtRu/CS and PtRu/VC, indicating that Ru atoms on the PtRu surface were gradually lost upon potential cycling. For all examined PtRu catalysts, the Cu oxidation curve from Pt sites in the potential region of 0.5−0.75 V increased during the early stage of the ADTs since more Pt sites exposed to the electrolyte after Ru atoms dissolved from the surface of the PtRu particles.

The surface Ru compositions calculated from Cu-stripping voltammograms recorded before and after the ADTs were compared for the examined PtRu catalysts. As shown in Figure 6d, the PtRu@CS catalyst demonstrated a suppressed Ru dissolution process compared to that of PtRu/CS and PtRu/VC. After 8000 repeated potential scans, the surface Ru atomic concentration for the PtRu@CS was still maintained at 40 at. %. Both PtRu/CS and PtRu/VC catalysts experienced serious surface Ru loss during the long-term ADTs since the surface Ru compositions dropped from the initial 66 at. % and 59 at. % to 19 at. % and 24 at. %, respectively. Therefore, the pore confined PtRu@CS catalyst exhibits a remarkably improved electrochemical stability against Ru dissolution; the enhanced electrochemical stability is ascribed to its unique structural characteristics, including the crystallinity, the high alloying degree (77%), and the nanopore confinement.

The evolution of ECSAs for each catalyst during the ADTs was demonstrated in Figure 7. Interestingly, the ECSA of PtRu@CS (86 m^2 g^{-1} of PtRu) kept increasing even up to 4000 initial potential scans. With further increasing the scanning cycles, the ECSA began to decrease, but over 90% of the initial ECSA was maintained after the ADTs. Similar results have been reported by Chen et al.[18] in characterizing the PtRu anode catalysts by methanol-stripping and CO-stripping experiments, in which the ECSA of their PtRu catalyst reached its maximum value after 1000 cycles and then began to decrease. It was speculated that the sudden dissolution of Ru at the beginning of degradation tests left many small voids, increasing the roughness and the surface area of the catalyst surface. The small voids gradually vanished with the continuing potential scans. The carbon corrosion on the PtRu catalyst surface during the ADTs gradually released more confined PtRu particles,

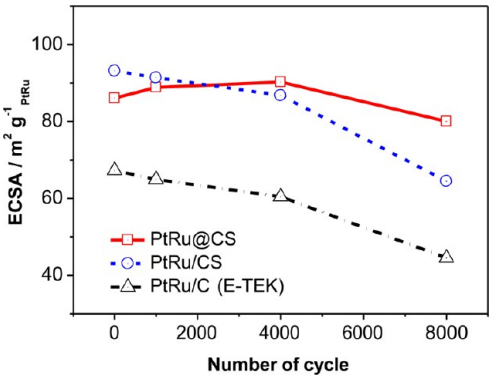

Figure 7. Change of ECSA estimated by Cu-stripping voltammetry for each PtRu catalyst during the ADTs.

which also contributed to the increase in ECSA at the initial stage of the ADTs.

3.3. Electrocatalytic Activity of the PtRu Catalysts. The difference in the nanostructures of the PtRu@CS and PtRu/CS catalysts is expected to induce different electrochemical properties. To characterize the variation of the catalytic properties of these PtRu catalysts toward MOR, we performed the cyclic voltammetry on the fresh and the degraded PtRu catalysts in 0.5 M H_2SO_4 solution containing 1.0 M CH_3OH before and after the ADTs. As shown in Figure 8a, the specific current peak at ca. 0.6−0.7 V in the forward scan is normally attributed to the catalytic activity for methanol oxidation. Both of the synthesized PtRu catalysts supported on HCMS carbon spheres exhibited higher initial catalytic activities than that of the commercial E-TEK catalyst (PtRu/VC). These improvements of the MOR activity could be attributed to the small particle size of PtRu nanoparticles and the hierarchical porous carbon supports which improve the mass transportation throughout the pores. Compared to the PtRu/CS catalyst, the PtRu@CS catalyst showed a relatively lower current and a positively shifted anodic peak in the methanol oxidation. This may suggest that pore confinement of PtRu nanoparticles imposed limitations on mass transportation and electrolyte accessibility to the surface of the metal catalysts.

After ADTs, all degraded PtRu catalysts behave like Pt/C catalysts, with anodic methanol oxidation peaks shifted positively for about 0.2 V. This indicates that the loss of Ru from the PtRu catalysts occurred during the ADTs. The mass-normalized current density at 0.6 V vs NHE of examined PtRu catalysts was compared before and after the ADTs: the current density of the PtRu@CS catalyst was slightly decreased from 56.3 to 51.5 mA $mg^{-1}_{\text{-PtRu}}$ after the ADTs, whereas the current densities of PtRu/CS and PtRu/VC faded from 70.1 to 30.8 mA $mg^{-1}_{\text{-PtRu}}$ and from 39.6 to 23.1 mA $mg^{-1}_{\text{-PtRu}}$, respectively. These results clearly suggested the superior electrochemical stability of the PtRu@CS catalyst to the PtRu/CS and the PtRu/VC.

In order to obtain more insights into the degradation behaviors of these PtRu bimetallic catalysts on nanoscale, SEM and TEM characterizations after the ADTs were performed (Figure 9). For the PtRu@CS catalyst, metal agglomerations can barely be observed either inside or outside the macroscopic hollow cores of the HCMS carbon spheres. The corresponding TEM image further confirmed that most of the metal particles were still trapped inside the mesoporous carbon shells and uniformly dispersed throughout the carbon structure. Moreover, the initial particle density distributed in the carbon textures was still well-maintained after the ADTs. However, the PtRu/CS and PtRu/VC catalysts underwent more severe degradations than the PtRu@CS catalyst since severe particle growth could be easily identified. These observations provide evidence that the uniform distribution and nanopore confinement of PtRu alloys in the porous structure of carbon support can significantly suppress the degradation processes such as metal particle agglomeration and detachment. EDX analysis on the decayed catalysts (Figure S6, Supporting Information) further confirmed that these observed agglomerated metal particles mainly consisted of Pt. This could also result from the leaching of Ru atoms during the ADTs.

3.4. Degradation Mechanisms of Carbon-Supported PtRu Catalysts. A variety of degradation mechanisms for carbon-supported Pt catalysts have been proposed in the literature.[53−56] It is generally accepted that the degradation of Pt nanocatalysts at high working potentials (at cathodes) involves the following four major processes: (i) coalescence via migration of Pt nanoparticles, (ii) particle growth via Ostwald ripening, (iii) detachment of Pt nanoparticles from carbon support, and (iv) dissolution and precipitation in the membrane.[54]

PtRu catalysts are substantially stable at the commonly used fuel cell anode potentials (0.2−0.3 V vs NHE), which is just slightly higher than hydrogen potential. However, for different reasons, the potential can overcome 0.5 V vs NHE. In this case, PtRu is not stable, and Ru dissolution can proceed. The degradation mechanisms of PtRu bimetallic catalysts became

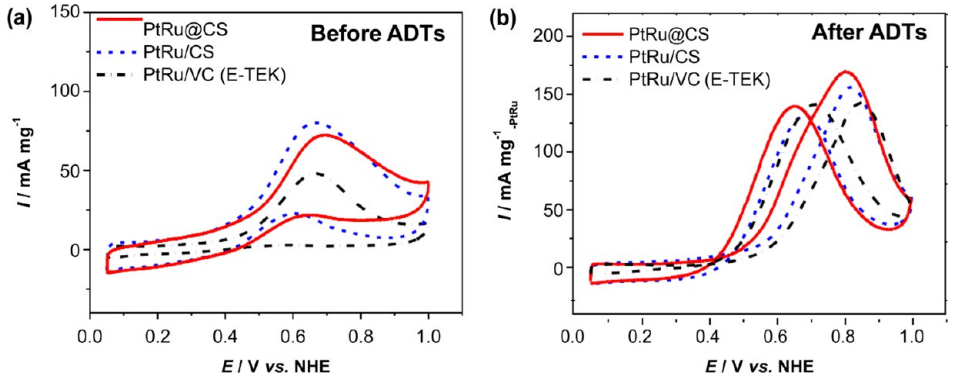

Figure 8. Cyclic voltammograms of the PtRu catalysts measured in 0.5 M H_2SO_4 and 1.0 M CH_3OH solution at a scan rate of 10 mV s^{-1} before (a) and after (b) the ADTs.

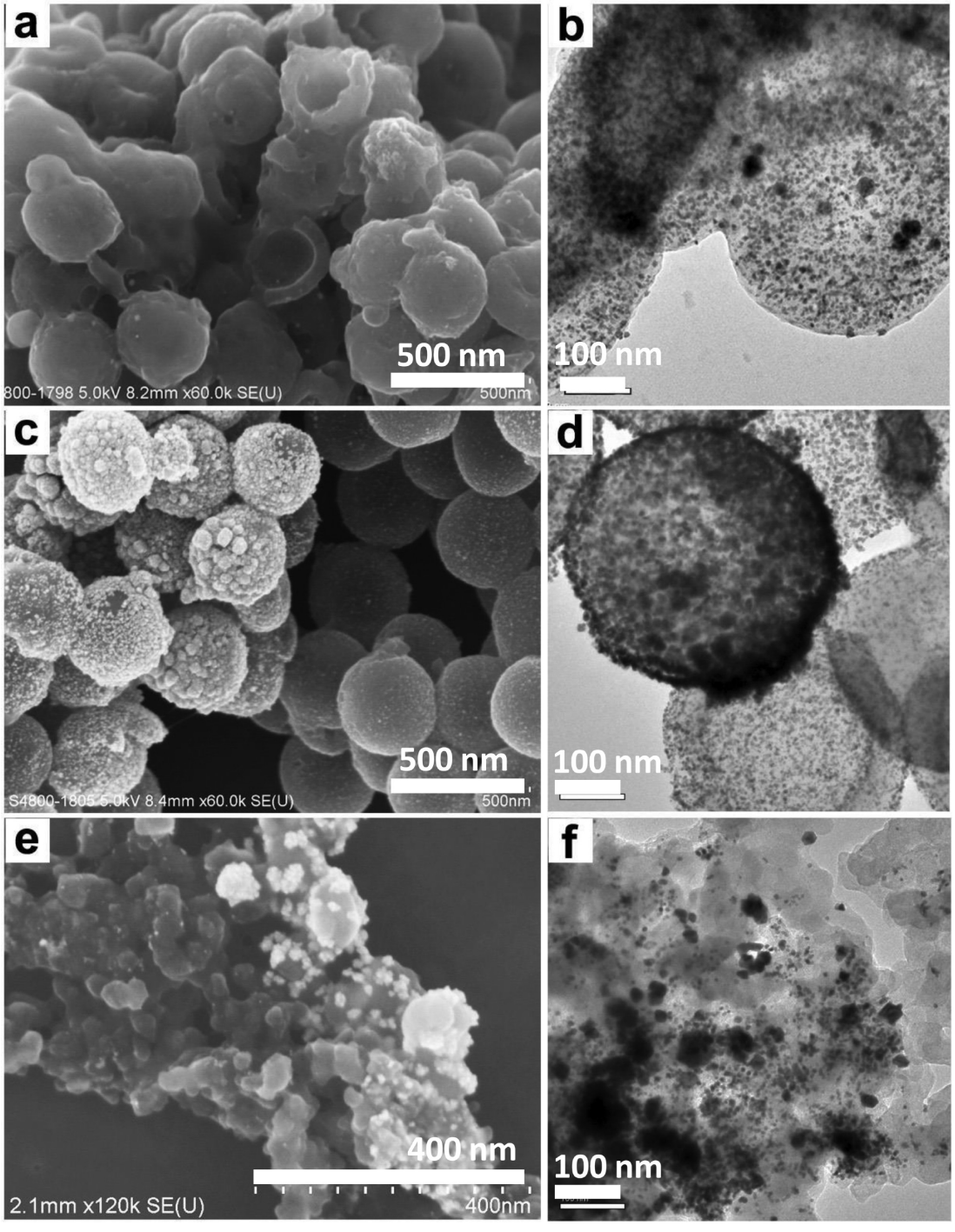

Figure 9. SEM and TEM images of the decayed PtRu catalysts after the ADTs: (a, b) for PtRu@CS, (c, d) for PtRu/CS, and (e, f) for PtRu/VC from E-TEK.

much more complex due to the presence of Ru. The simultaneous dissolution of Pt and Ru atoms takes place on the catalyst surface, followed by subsequent redeposition of dissolved Pt species without Ru.[10] In addition to the dealloying of Ru, other degradation processes, such as particle growth via agglomeration, also lead to the loss of ECSA and the decrease in activity. As illustrated in Scheme 1, the PtRu@CS catalyst enables a high alloying degree and a uniform distribution of PtRu nanoalloys in carbon texture, whereas the PtRu/CS catalyst is located on the external surface of the carbon support with a core−shell microstructure. Such differences in PtRu crystallinity and particle depositions would significantly affect their electrochemical stabilities and degradation behaviors.

(i). Ru Dissolution. As we mentioned before, a major challenge for improving the electrochemical stability of PtRu catalysts is to suppress Ru dissolution from the catalyst surface.[10,17] For the PtRu@CS catalyst, the PtRu nanoalloys were confined in carbon structures and partially exposed to the electrolyte. During the long-term ADTs, Ru dissolution only occurred at the exposed surface, leading to a few layers of the outmost alloy surface being dealloyed, whereas the rest was still well protected by the carbon nanopores. The formed Pt skin

layer also has a role to protect further dealloying of Ru from the inside. As to the PtRu/CS and PtRu/VC catalysts, Ru dissolution took place at the Ru-rich surface which was fully exposed to the electrolyte at a fast rate at the initial stage of ADTs. Besides, the high alloying degree of the PtRu nanoparticles (77%) benefitting from the high-temperature postheat-treatment process also contributes to suppress the Ru dissolution process.

(ii). Particle Growth and Agglomeration. For the PtRu@CS catalyst, most of the PtRu alloys were confined in the carbon nanopores and dispersed throughout the hierarchical carbon texture. The porous structure of the carbon support could limit their growth and agglomeration. As observed from the TEM image of the degraded catalyst, most metal particles in the PtRu@CS catalyst were still trapped inside the mesoporous carbon shells after ADTs, whereas significant particle agglomeration was observed for both PtRu/CS and PtRu/VC catalysts. The obvious TEM contrasts clearly suggested that confining PtRu NPs in mesoporous carbon texture limit the movement of the metal nanoparticles and thereby suppress the degradation process via the particle agglomeration.

Considering that traditional DMFCs are normally operated at increased temperature (up to 60 °C) for achieving maximum power density, the Ru dissolution problem could be more serious in practical DMFCs than in this study (24 °C). We therefore believe that the strategy demonstrated here by employing the particle pore-confinement effect to address the Ru dissolution problem can be more promising in the practical applications of DMFCs.

However, it is also worth mentioning that the pore confinement of PtRu nanoparticles in the porous carbon structure also has negative aspects, such as poor utilization of the costly PtRu catalysts and the mass transfer limitations. These factors may lead to large voltage polarizations at high current densities and hence affect the power performance of the fuel cell.

4. CONCLUSIONS

In summary, we have demonstrated a surfactant-free route to prepare a stable PtRu electrocatalyst for methanol oxidation. The PtRu particles were highly alloyed and uniformly dispersed throughout the porous carbon structure. Compared to the samples prepared from the traditional ways, the newly developed catalyst exhibited a more stable electrochemical performance toward MOR and less leaching of Ru species during the operation. Both of the alloying degree and pore confinement of PtRu nanoparticles play important roles in mitigating Ru dissolution from the catalyst surface; moreover, the pore-confinement effect can effectively prevent particle agglomeration and migration, resulting in a stable ECSA. We believe that the synthetic strategy demonstrated here can also be extended to prepare other carbon-supported mixed-metal electrocatalysts with durable electrochemical performance.

■ ASSOCIATED CONTENT

Supporting Information

SEM and TEM characterizations for SCMS silica spheres and the replicated carbon spheres, N_2 sorption analysis of silica spheres, and EDX analysis of the degraded catalysts. This material is available free of charge via the Internet at http://pubs.acs.org.

■ AUTHOR INFORMATION

Corresponding Author

*E-mail: chunzhenxp@gmail.com.

Notes

The authors declare no competing financial interest.

■ ACKNOWLEDGMENTS

The author thanks the Electron Microscope Unit of The University of Hong Kong for offering help on the TEM and SEM characterizations.

■ ABBREVIATIONS

ADT, accelerating degradation test; DMFC, direct methanol fuel cell; ECSA, electrochemically active surface area; MOR, methanol oxidation reaction; NP, nanoparticle; ORR, oxygen reduction reaction

■ REFERENCES

(1) Yu, W.; Porosoff, M. D.; Chen, J. G. Review of Pt-Based Bimetallic Catalysis: From Model Surfaces to Supported Catalysts. *Chem. Rev.* **2012**, *112* (11), 5780−5817.

(2) Wei, Z.; Sun, J.; Li, Y.; Datye, A. K.; Wang, Y. Bimetallic catalysts for hydrogen generation. *Chem. Soc. Rev.* **2012**, *41* (24), 7994.

(3) Zhao, X.; Yin, M.; Ma, L.; Liang, L.; Liu, C. P.; Liao, J. H.; Lu, T. H.; Xing, W. Recent advances in catalysts for direct methanol fuel cells. *Energ Environ. Sci.* **2011**, *4* (8), 2736−2753.

(4) Rabis, A.; Rodriguez, P.; Schmidt, T. J. Electrocatalysis for Polymer Electrolyte Fuel Cells: Recent Achievements and Future Challenges. *ACS Catal.* **2012**, *2* (5), 864−890.

(5) Toda, T. Enhancement of the Electroreduction of Oxygen on Pt Alloys with Fe, Ni, and Co. *J. Electrochem. Soc.* **1999**, *146* (10), 3750.

(6) Stamenkovic, V. R.; Fowler, B.; Mun, B. S.; Wang, G. F.; Ross, P. N.; Lucas, C. A.; Markovic, N. M. Improved oxygen reduction activity on Pt3Ni(111) via increased surface site availability. *Science* **2007**, *315* (5811), 493−497.

(7) Hwang, S. J.; Kim, S. K.; Lee, J. G.; Lee, S. C.; Jang, J. H.; Kim, P.; Lim, T. H.; Sung, Y. E.; Yoo, S. J. Role of electronic perturbation in stability and activity of pt-based alloy nanocatalysts for oxygen reduction. *J. Am. Chem. Soc.* **2012**, *134* (48), 19508−11.

(8) Sasaki, K.; Naohara, H.; Choi, Y.; Cai, Y.; Chen, W. F.; Liu, P.; Adzic, R. R. Highly stable Pt monolayer on PdAu nanoparticle electrocatalysts for the oxygen reduction reaction. *Nat. Commun.* **2012**, *3*, 1115.

(9) Bonakdarpour, A.; Löbel, R.; Atanasoski, R. T.; Vernstrom, G. D.; Schmoeckel, A. K.; Debe, M. K.; Dahn, J. R. Dissolution of Transition Metals in Combinatorially Sputtered $Pt_{1-x-y}M_xM_y'$ (M, M′=Co, Ni, Mn, Fe) PEMFC Electrocatalysts. *J. Electrochem. Soc.* **2006**, *153* (10), A1835.

(10) Antolini, E. The problem of Ru dissolution from Pt-Ru catalysts during fuel cell operation: analysis and solutions. *J. Solid State Electr.* **2011**, *15* (3), 455−472.

(11) Holton, O. T.; Stevenson, J. W. The Role of Platinum in Proton Exchange Membrane Fuel Cells. *Platinum Met. Rev.* **2013**, *57* (4), 259−271.

(12) Andersen, S. M.; Grahl-Madsen, L.; Skou, E. M. Studies on PEM fuel cell noble metal catalyst dissolution. *Solid State Ionics* **2011**, *192* (1), 602−606.

(13) Roth, C.; Benker, N.; Theissmann, R.; Nichols, R. J.; Schiffrin, D. J. Bifunctional electrocatalysis in Pt-Ru nanoparticle systems. *Langmuir* **2008**, *24* (5), 2191−2199.

(14) Roth, C.; Papworth, A. J.; Hussain, I.; Nichols, R. J.; Schiffrin, D. J. A Pt/Ru nanoparticulate system to study the bifunctional mechanism of electrocatalysis. *J. Electroanal. Chem.* **2005**, *581* (1), 79−85.

(15) Liu, J. G.; Zhou, Z. H.; Zhao, X. X.; Xin, Q.; Sun, G. Q.; Yi, B. L. Studies on performance degradation of a direct methanol fuel cell (DMFC) in life test. *Phys. Chem. Chem. Phys.* **2004**, *6* (1), 134−137.
(16) Inaba, M. Durability of Electrocatalysts in Polymer Electrolyte Fuel Cells. *ECS Trans.* **2009**, 573−581.
(17) Yamada, H.; Shimoda, D.; Matsuzawa, K.; Tasaka, A.; Inaba, M. Stability of Pt- Ru/C Catalysts: Effects of Ru Content. *ECS Trans.* **2007**, *11*, 325−334.
(18) Chen, W. M.; Sun, G. Q.; Liang, Z. X.; Mao, Q.; Li, H. Q.; Wang, G. X.; Xin, Q.; Chang, H.; Pak, C. H.; Seung, D. Y. The stability of a PtRu/C electrocatalyst at anode potentials in a direct methanol fuel cell. *J. Power Sources* **2006**, *160* (2), 933−939.
(19) Shyam, B.; Arruda, T. M.; Mukerjee, S.; Ramaker, D. E. Effect of RuOxHy Island Size on PtRu Particle Aging in Methanol. *J. Phys. Chem. C* **2009**, *113* (45), 19713−19721.
(20) Piela, P.; Eickes, C.; Brosha, E.; Garzon, F.; Zelenay, P. Ruthenium crossover in direct methanol fuel cell with Pt-Ru black anode. *J. Electrochem. Soc.* **2004**, *151* (12), A2053−A2059.
(21) Joghee, P.; Pylypenko, S.; Olson, T.; Dameron, A.; Corpuz, A.; Dinh, H. N.; Wood, K.; O'Neill, K.; Hurst, K.; Bender, G.; Gennett, T.; Pivovar, B.; O'Hayre, R. Enhanced Stability of PtRu Supported on N-Doped Carbon for the Anode of a DMFC. *J. Electrochem. Soc.* **2012**, *159* (11), F768−F778.
(22) Li, Y.; Zhu, E.; McLouth, T.; Chiu, C. Y.; Huang, X.; Huang, Y. Stabilization of high-performance oxygen reduction reaction pt electrocatalyst supported on reduced graphene oxide/carbon black composite. *J. Am. Chem. Soc.* **2012**, *134* (30), 12326−9.
(23) Maiyalagan, T.; Alaje, T. O.; Scott, K. Highly Stable Pt-Ru Nanoparticles Supported on Three-Dimensional Cubic Ordered Mesoporous Carbon (Pt-Ru/CMK-8) as Promising Electrocatalysts for Methanol Oxidation. *J. Phys. Chem. C* **2012**, *116* (3), 2630−2638.
(24) Maiyalagan, T. Silicotungstic acid stabilized Pt-Ru nanoparticles supported on carbon nanofibers electrodes for methanol oxidation. *Int. J. Hydrogen Energy* **2009**, *34* (7), 2874−2879.
(25) Park, Y.; Lee, B.; Kim, C.; Oh, Y.; Nam, S.; Park, B. The effects of ruthenium- oxidation states on Ru dissolution in PtRu thin-film electrodes. *J. Mater. Res.* **2009**, *24* (9), 2762−2766.
(26) Gancs, L.; Hakim, N.; Hult, B.; Mukerjee, S. Dissolution of Ru from PtRu Electrocatalysts and its Consequences in DMFCs. *ECS Trans.* **2006**, *3*, 607−618.
(27) Hyun, M. S.; Kim, S. K.; Lee, B.; Peck, D.; Shul, Y.; Jung, D. Effect of NaBH4 concentration on the characteristics of PtRu/C catalyst for the anode of DMFC prepared by the impregnation method. *Catal. Today* **2008**, *132* (1−4), 138−145.
(28) Bensebaa, F.; Patrito, N.; Le Page, Y.; L'Ecuyer, P.; Wang, D. S. Tunable platinum-ruthenium nanoparticle properties using microwave synthesis. *J. Mater. Chem.* **2004**, *14* (22), 3378−3384.
(29) Liu, Z. L.; Ling, X. Y.; Su, X. D.; Lee, J. Y. Carbon-supported Pt and PtRu nanoparticles as catalysts for a direct methanol fuel cell. *J. Phys. Chem. B* **2004**, *108* (24), 8234−8240.
(30) Sau, T. K.; Lopez, M.; Goia, D. V. Method for Preparing Carbon Supported Pt-Ru Nanoparticles with Controlled Internal Structure. *Chem. Mater.* **2009**, *21* (15), 3649−3654.
(31) Bock, C.; Paquet, C.; Couillard, M.; Botton, G. A.; MacDougall, B. R. Size-Selected Synthesis of PtRu Nano-Catalysts: Reaction and Size Control Mechanism. *J. Am. Chem. Soc.* **2004**, *126* (25), 8028−8037.
(32) Lee, D.; Hwang, S.; Lee, I. One-step preparation and characterization of PtRu (1:1)/C electrocatalysts by polyol method for polymer electrolyte fuel cells. *J. Power Sources* **2006**, *160* (1), 155−160.
(33) Rojas, S.; Garcia-Garcia, F. J.; Jaras, S.; Martinez-Huerta, M. V.; Fierro, J. L. G.; Boutonnet, M. Preparation of carbon supported Pt and PtRu nanoparticles from microemulsion - Electrocatalysts for fuel cell applications. *Appl. Catal. A-Gen.* **2005**, *285* (1−2), 24−35.
(34) Zhang, X.; Chan, K. Y. Water-in-oil microemulsion synthesis of platinum-ruthenium nanoparticles, their characterization and electrocatalytic properties. *Chem. Mater.* **2003**, *15* (2), 451−459.
(35) Tu, H. C.; Wang, W. L.; Wan, C. C.; Wang, Y. Y. Novel method for the synthesis of hydrophobic Pt-Ru nanoparticles and its application to preparing a nafion-free anode for the direct methanol fuel cell. *J. Phys. Chem. B* **2006**, *110* (32), 15988−15993.
(36) Xue, X. Z.; Lu, T. H.; Liu, X. P.; Xing, W. Simple and controllable synthesis of highly dispersed Pt-Ru/C catalysts by a two-step spray pyrolysis process. *Chem. Commun.* **2005**, *12*, 1601−1603.
(37) Liu, S. H.; Yu, W. Y.; Chen, C. H.; Lo, A. Y.; Hwang, B. J.; Chien, S. H.; Liu, S. B. Fabrication and characterization of well-dispersed and highly stable PtRu nanoparticles on carbon mesoporous material for applications in direct methanol fuel cell. *Chem. Mater.* **2008**, *20* (4), 1622−1628.
(38) Gurau, B.; Viswanathan, R.; Liu, R. X.; Lafrenz, T. J.; Ley, K. L.; Smotkin, E. S.; Reddington, E.; Sapienza, A.; Chan, B. C.; Mallouk, T. E.; Sarangapani, S. Structural and electrochemical characterization of binary, ternary, and quaternary platinum alloy catalysts for methanol electro-oxidation. *J. Phys. Chem. B* **1998**, *102* (49), 9997−10003.
(39) Yan, X. P.; Liu, H. F.; Liew, K. Y. Size control of polymer-stabilized ruthenium nanoparticles by polyol reduction. *J. Mater. Chem.* **2001**, *11* (12), 3387−3391.
(40) Antolini, E.; Cardellini, F. Formation of carbon supported PtRu alloys: an XRD analysis. *J. Alloys Compd.* **2001**, *315* (1−2), 118−122.
(41) Takenaka, S.; Matsumori, H.; Matsune, H.; Kishida, M. Highly durable Pt cathode catalysts for polymer electrolyte fuel cells; coverage of carbon black-supported Pt catalysts with silica layers. *Appl. Catal. A-Gen.* **2011**, *409*, 248−256.
(42) Galeano, C.; Meier, J. C.; Peinecke, V.; Bongard, H.; Katsounaros, I.; Topalov, A. A.; Lu, A. H.; Mayrhofer, K. J. J.; Schuth, F. Toward Highly Stable Electrocatalysts via Nanoparticle Pore Confinement. *J. Am. Chem. Soc.* **2012**, *134* (50), 20457−20465.
(43) Green, C. L.; Kucernak, A. Determination of the platinum and ruthenium surface areas in platinum-ruthenium electrocatalysts by underpotential deposition of copper. 2. Effect of surface composition on activity. *J. Phys. Chem. B* **2002**, *106* (44), 11446−11456.
(44) Green, C. L.; Kucernak, A. Determination of the platinum and ruthenium surface areas in platinum-ruthenium alloy electrocatalysts by underpotential deposition of copper. I. Unsupported catalysts. *J. Phys. Chem. B* **2002**, *106* (5), 1036−1047.
(45) Li, F. J.; Chan, K. Y.; Yung, H. Carbonization over PFA-protected dispersed platinum: an effective route to synthesize high performance mesoporous-carbon supported Pt electrocatalysts. *J. Mater. Chem.* **2011**, *21* (32), 12139−12144.
(46) Qi, J.; Jiang, L. H.; Wang, S. L.; Sun, G. Q. Synthesis of graphitic mesoporous carbons with high surface areas and their applications in direct methanol fuel cells. *Appl. Catal. B: Environ.* **2011**, *107* (1−2), 95−103.
(47) Antolini, E.; Cardellini, F.; Giorgi, L.; Passalacqua, E. Effect of Me (Pt plus Ru) content in Me/C catalysts on PtRu alloy formation: An XRD analysis. *J. Mater. Sci. Lett.* **2000**, *19* (23), 2099−2103.
(48) Choi, K.-H.; Lee, K.-S.; Jeon, T.-Y.; Park, H.-Y.; Jung, N.-G.; Chung, Y.-H.; Sung, Y.-E. High Alloying Degree of Carbon Supported Pt-Ru Alloy Nanoparticles Applying Anhydrous Ethanol as a Solvent. *J. Electrochem. Sci. Technol.* **2010**, *1* (1), 19−24.
(49) Vegard, L. Z. *Physics* **1921**, *5*, 17−26.
(50) Radmilovic, V.; Gasteiger, H. A.; Ross, P. N. Structure and Chemical-Composition of a Supported Pt-Ru Electrocatalyst for Methanol Oxidation. *J. Catal.* **1995**, *154* (1), 98−106.
(51) Onodera, T.; Suzuki, S.; Takamori, Y.; Daimon, H. Improved methanol oxidation activity and stability of well-mixed PtRu catalysts synthesized by electroless plating method with addition of chelate ligands. *Appl. Catal. A: Gen.* **2010**, *379* (1−2), 69−76.
(52) Shao, Y. Y.; Kou, R.; Wang, J.; Viswanathan, V. V.; Kwak, J. H.; Liu, J.; Wang, Y.; Lin, Y. H. The influence of the electrochemical stressing (potential step and potential-static holding) on the degradation of polymer electrolyte membrane fuel cell electrocatalysts. *J. Power Sources* **2008**, *185* (1), 280−286.
(53) Meier, J. C.; Galeano, C.; Katsounaros, I.; Topalov, A. A.; Kostka, A.; Schuth, F.; Mayrhofer, K. J. J. Degradation Mechanisms of

Pt/C Fuel Cell Catalysts under Simulated Start-Stop Conditions. *ACS Catal.* **2012**, *2* (5), 832−843.
(54) Shao-Horn, Y.; Sheng, W. C.; Chen, S.; Ferreira, P. J.; Holby, E. F.; Morgan, D. Instability of supported platinum nanoparticles in low-temperature fuel cells. *Top Catal.* **2007**, *46* (3−4), 285−305.
(55) Virkar, A. V.; Zhou, Y. K. Mechanism of catalyst degradation in proton exchange membrane fuel cells. *J. Electrochem. Soc.* **2007**, *154* (6), B540−B547.
(56) Topalov, A. A.; Katsounaros, I.; Auinger, M.; Cherevko, S.; Meier, J. C.; Klemm, S. O.; Mayrhofer, K. J. Dissolution of platinum: limits for the deployment of electrochemical energy conversion? *Angew. Chem., Int. Ed. Engl.* **2012**, *51* (50), 12613−5.